ISDN 1039-3218

Sediment Characteristics in Port Phillip Bay

P. Greilach, Z. You, K. Black and R. Gorman
Marine and Freshwater Resources Institute
115 Victoria Parade, Fitzroy, Victoria Australia

Locked Bag 7, Collins Street East Post Office
Melbourne 8003, Australia

Technical Report No.23

Port Phillip Bay Environmental Study
CSIRO Environmental Projects Office

PO Box 225, Dickson, ACT 2602, Australia

March 1997

EXECUTIVE SUMMARY

Nutrients and toxicants in marine systems are often closely related to suspended and bed sediments. An understanding of sediment characteristics and sedimentary transport processes was an important component in the development of transport and integrated models of Port Phillip Bay. The Victorian Institute of Marine Sciences (VIMS), now operating as part of the Marine and Freshwater Resources Institute (MAFRI), was commissioned to collect and analyse data on undisturbed bed sediments in Port Phillip Bay.

Core samples were collected from the seabed at 80 sites throughout Port Phillip Bay, and analysed for a variety of physical properties of importance in the transport processes of bed sediments.

Grain sizes were measured by fall velocity techniques. They displayed a distribution of fine muddy sediments in the Central Bay and Geelong Arm, with coarser material predominating at sites nearer shore.

Sediment and bulk densities in the top 5 cm of the core samples showed wide variation between sampling sites, as did the derived properties of water content, void ratio and porosity. Low densities were noted at the Central Bay and Geelong Arm sites. A limited number of measurements deeper in cores showed little consistent pattern in the depth variation of sediment and bulk density, but the water content and void ratio were both found to decrease with depth.

Permeabilities ranged from 1 to 0.0003 mm/s, the highest values occurring at central Bay sites with relatively fine grain sizes. No significant correlation was found between permeability and either grain size or porosity.

Viscosity measurements were made on samples from the top 5 cm at 46 of the sites. Flow curves typically showed higher shear stresses on the down-ramps than on the up-ramps. Yield stresses from 7 to 400 Pa were obtained.

TABLE OF CONTENTS

LIST OF TABLES

Page No.

LIST OF FIGURES

Page No.

1. INTRODUCTION

Nutrient and toxicant processes in marine systems are often closely related to suspended and bed sediments. An understanding of sediment characteristics and sedimentary transport processes were therefore important components in the development of transport and integrated models of Port Phillip Bay. As part of the Port Phillip Bay Environmental Study, the Victorian Institute of Marine Sciences (VIMS), now part of the Marine and Freshwater Resources Institute (MAFRI) was commissioned to collect and analyse data on sediments in Port Phillip Bay. The first phase of this project, the collection and analysis of undisturbed bed sediment samples, is the subject of this report.

The objective was to determine physical properties of sediments such as physical composition, particle size distribution, density, porosity, moisture content, viscosity, consolidation and hydraulic permeability from a large number of sites throughout the Bay.

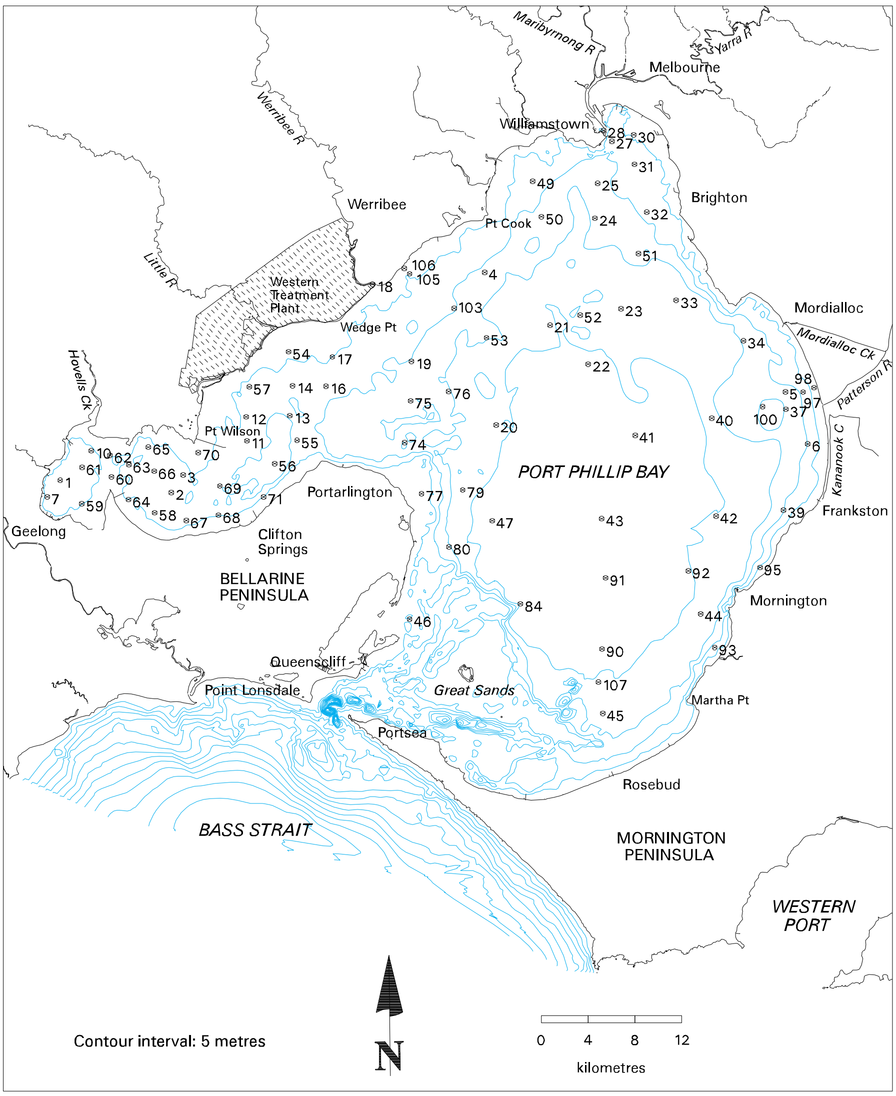

Sediment Samples Locality Map - 16/9/96

Figure 1: Map of Port Phillip Bay showing core sampling sites.

2. METHODS

2.1. Collection and preparation of cores

Three sediment cores from each of 80 sites in Port Phillip Bay (Figure 1) were collected by teams of three divers over the period 9/3/94 to 22/4/94. Water depths were measured by an acoustic echo sounder (*SR85*, AWA Marine, Japan). Positions were determined by a Differential Global Positioning System.

Sediment cores were collected using 100 mm diameter PVC tubes approximately 400 mm long. The tubes were driven into the substrate either by hand or by hammer depending on the hardness of the substrate. Prior to withdrawal from the sediment PVC caps were placed over both the top and bottom of the tubes. In hard substrates the area around the tube was excavated by hand to make room for the application of the bottom cap whilst maintaining the integrity of the core. Cores were transported to the surface in an upright position where the bottom cap was secured by adhesive tape. The tubes were labelled then frozen in an upright position.

In the laboratory, one core sample from each site was placed upright in a water bath to which hot water was added until the depth of water was just below the end cap of the tube. The core remained in the water bath for a period sufficient to allow the outer edge of the core to begin to liquefy (between 1-3 minutes depending on the core material). The core was then removed from the tube and placed on a clean white plastic tray. Using a hammer and flat chisel the core was carefully halved lengthways to expose the core cross-section and the remnant ice on the top of the core was removed. The split cores were then photographed next to a metre rule in natural light to minimise colour distortion in the resulting pictures.

The length of the cores was measured and the depth of obvious colour bands in each core was noted. Each of the colour bands was matched against a Munsell soil colour chart and the Munsell reference and colour description also noted. A qualitative description of the sediment type of each band was made, including the amount of shell. These records are available from MAFRI.

The core was then sub-divided for further analysis, with three sub-samples being taken as follows:

TOP	0 to 5 cm depth of core to be used for viscosity analysis and density analysis;
BOTTOM	5 to 10 cm depth of core to be used for grain size analysis; and
CONSOL	cross-section of 0 to 10cm of core to be used for consolidation analysis.

These sub-samples were then stored in small air-tight jars and topped up with sea water to prevent dehydration and destruction of floccules. The samples were then re-frozen to maintain their water content.

2.2. Permeability Analysis

A single core from each of 76 sites was used for the permeability analysis. The permeability chamber (Figure 2) was prepared prior to the analysis of each core with particular attention paid to the condition of O-rings. A perforated support was placed in the chamber to prevent sediment falling into the bottom of the chamber thereby decreasing the effective volume of core through which water could permeate. The assembled chamber was filled with sea water prior to inserting the core so that no air pockets could form and affect the flow rate of water through the chamber. Sea water was used throughout the experiment to ensure that salinities would be similar to those occurring within the environment of Port Phillip Bay.

To enable the frozen core to be extracted from the PVC tube it was placed in a hot water bath and defrosted until its outer edge began to liquefy. The core was removed from the PVC tube and cut to a length of 20 cm. Excess core was removed from the bottom. If the core was shorter than 20 cm the length of the core (L in Figure 2) was noted so that it could be accounted for in the calculation of the permeability constant. The core was then placed into the permeability chamber, ensuring that no air bubbles were trapped under it. Additional sea water was added to cover the core and prevent de-hydration. Following this, the core was allowed to defrost overnight at room temperature.

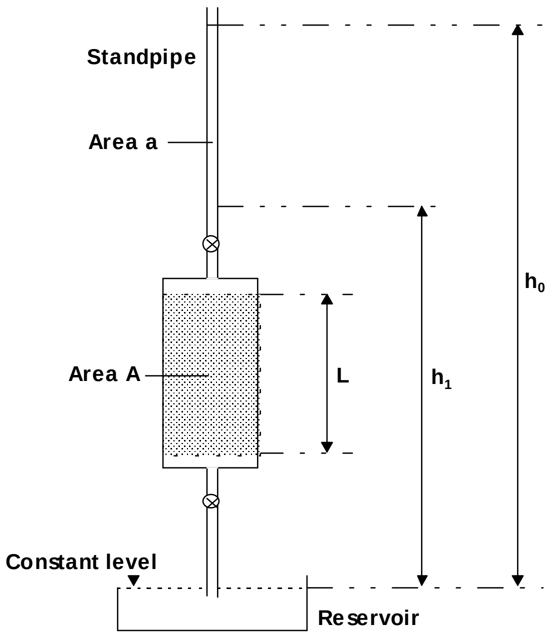

Figure 2: Falling-head permeability chamber used to measure the coefficient of permeability of cohesive sediments.

Prior to analysis the seal of sediment against the wall of tube was checked and, if necessary, the sediment was packed by stirring gently at the edges to improve the seal. In such cases the core was again left to settle overnight. As a rule of thumb, fine sand was not stirred because this caused sediment to fall through the support plate. Darcy's Law assumes that the sample has an approximately uniform density, time history and structure but the action of stirring may have altered the original structure of some samples.

Once a core was ready for analysis, the permeability chamber was topped up with sea water and its lid screwed on. The marked upper tube (stand pipe) was then filled with sea water and vented to zero level (1.8 m above the lower reservoir). The tube running from the chamber to the lower reservoir was placed in the lower reservoir and the initial time and height (h_0) recorded. The taps were then opened to allow water flow to occur between the upper and lower reservoirs (through the core). After either the level of water in the upper reservoir had dropped by approximately 90 cm or the time since start had reached 15-20 minutes, the taps were closed and the final height (h_1) and time recorded.

2.3. Consolidation Analysis

The CONSOL (0 - 10 cm) sub-samples were placed in a graduated 1L cylinder, which was then filled with sea water to approximately 700 mL volume and the exact level recorded. The cylinder was then sealed tightly with a rubber stopper and thoroughly shaken. The sample was then observed as it settled and the position of the sediment interface recorded at intervals of 5, 10 and 15 minutes and 1, 4 and 24 hours. After this was complete, each of the samples was photographed *in vitro*.

2.4. Viscosity Analysis

Sediment core TOP (0 - 5 cm) sub-samples from 46 sites were tested for their viscosity properties using a HAAKE Rotoviscometer. A sample was placed into the gap between the inner cylinder sensor and cup and held at a constant temperature by a temperature control unit. A motor drove the inner cylinder at various selected rates resulting in a viscosity related torque caused by the resistance of the sample to shearing. The measure of deflection of a spring correlates linearly with the torque. The spring deflection is transformed into an electrical signal and is displayed as a digital read-out on the Rotovisco RV20 recorder.

The instrument defined a flow curve for each tested sample. The flow curve shows the relationship between the shear stress and the shear rate; that is, the change in velocity with radius across the sample.

Analyses were only performed on TOP sub-samples that were of fine grain size (e.g. clays, muds and/or fine sands). Sub-samples with medium to coarse grain size or of high shell fragment content were found to jam the viscometer apparatus or give rise to erratic and uninterpretable results. Out of the possible 80 TOP samples only 46 were tested for their viscosity properties.

Prior to testing, each TOP sample was completely thawed, mixed and left to resettle. Excess water (i.e. water above the sediment line in the sample jar) was drawn off with a pipette without disturbing or accidentally removing any of the sediment itself. A small portion of the sample was then spooned into the sensor system cup, the cup re-mounted into the viscometer apparatus and the viscosity test started.

A reading for τ (shear stress) was made for each incremental step up and down through the 10 possible D (shear rate) selections. A 15 second interval at each shear rate setting allowed the readings to settle prior to recording the τ value. A further three minute interval between the end of the "loading" (up-ramp) and beginning of the "unloading" (down-ramp) shear rate selections allowed the sample to equilibrate between stages of increasing and decreasing shear stress. This facilitated determination of the asymptotic shear stress value for the sample.

2.5. Grain Size Analysis

An automated settling tube system was used to conduct a grain size analysis of the core samples. The system consists of two perspex settling tubes; a 1.9 m long tube for processing the coarse fraction (sediment diameter greater than 45 micron) and a 20 cm tube for processing the fine fraction (sediment diameter less than 45 micron). Approximately 10 g of BOTTOM (5 - 10 cm) sediment was washed through a 45 μm sieve using fresh water to remove any mud sized particles and processed in the 1.9 m settling tube. A further 10 g of unwashed sediment was processed in the 20 cm tube to reduce collecting times for the fine fraction.

A collection plate near the base of the tube hangs below an electronic balance. The sediment samples were released from a spinning disc near the top of the tube, which spread sediment uniformly across the water column. The weight of sediment arriving at the collection plate was transmitted via an RS-232 interface on the balance to a computer.

The results from the two tubes were merged, correcting for the different weights of the coarse and fine fractions and the different temperatures and salinities of the water in the two tubes. The merging procedure normalised the mass of sediment processed through the longer settling tube to the mass of sediment processed through the small settling tube. Potential errors arising from short duration vortices in the small settling tube could be eliminated whilst providing better resolution of the distribution of large particles in each sample. An Excel interface produced the graphics, statistical measures and a textural description of the sample.

The use of a two tube system enables direct comparison of fine and coarse fractions, which is not readily possible if the traditional method of analysing the fine fraction using a pipette is employed. Small errors associated with release times can also be completely eliminated after digital merging of the relevant sections of the output files.

The two main causes of measurement error in settling tube analysis are wall effects and clumping of sediment. The former was overcome by selecting a 40 cm diameter tube to minimise wall interaction, and by making the collection plate considerably smaller than the tube diameter so that material near the walls was not collected. Clumping was reduced by the utilisation of a spinning disc release system that provides minimal turbulence, and by selecting a sample size in the range ~1-10 g so as to minimise grain/grain interactions and sample error.

The settling tube system is calibrated using glass beads of known size and density to ensure that measurements of grain size are accurate (Black and Rosenberg, 1991).

2.6. Density Analysis

TOP (0 - 5 cm) sediment were used for density measurements. A section was cut from the frozen core and weighed. The volume of the frozen sample was measured by misplacement in a measuring cylinder. The sample was then dried in an oven at 90°-100°C and subsequently re-weighed. Comparing the two masses provided the mass of water in the sample, and hence the volume of water in the liquid state, assuming a density of 1025 kg/m^3. Densities of the whole sample and of its sediment content could then be calculated, correcting for the difference in density of liquid and frozen water.

3. RESULTS AND DISCUSSION

3.1. Permeability

The permeabilities (*k*) measured at 76 sites in Port Phillip Bay are presented in Table 1. The values found range over more than three orders of magnitude, from 3×10^{-7} to nearly 10^{-3} m/s. Figure 3 shows the spatial distribution of permeability within Port Phillip Bay. Sites with particularly high permeability are located in the central to southern Bay, and near the mouth of the Yarra River.

The texture and porosity of a collected sample are the primary factors affecting permeability if other factors such as temperature, viscosity of the fluid and the degree of saturation of the sample are fixed during testing. Figure 4 shows the variation of permeability with grain size and porosity. It can be seen that the data show little evidence that the permeability is primarily dependent on either grain size or porosity in the present study. The reason for this is not known.

It was of interest to investigate the variation of permeability (*k*) with the void ratio (*e*) since the assumption of $k = k(e)$ has been adopted in consolidation theory. Figure 5 indicates that the data do not support this assumption.

Table 1: Core permeabilities (*k*) by site indicating the permeability dependent sediment classification

site	core length (m)	initial time	final time	initial height (cm)	final height (cm)	k (m/s)	class
1	0.2	12:33:56	12:35:15	0	90	8.56E-05	v. fine sand, clay laminate
2	0.2	10:57:27	11:06:16	0	90	1.28E-05	v. fine sand, clay laminate
3	0.2	9:59:20	10:06:51	0	85	1.38E-05	v. fine sand, clay laminate
4	0.2	10:29:09	10:30:09	0	90	1.13E-04	clean sands
5	0.2	12:11:39	12:23:12	0	90	9.75E-06	v. fine sand, clay laminate
6	0.2	12:20:20	12:41:56	0	90	5.22E-06	v. fine sand, clay laminate
7	0.2	14:22:50	14:29:52	0	90	1.60E-05	v. fine sand, clay laminate
10	0.2	10:11:04	10:16:04	0	90	2.25E-05	v. fine sand, clay laminate
11	0.2	15:03:28	15:23:06	0	55	3.03E-06	v. fine sand, clay laminate
12	0.14	12:13:25	12:14:54	0	90	5.32E-05	v. fine sand, clay laminate
13	0.2	15:47:24	16:17:51	0	90	3.70E-06	v. fine sand, clay laminate
14	0.2	11:09:04	11:38:15	0	90	3.86E-06	v. fine sand, clay laminate
16	0.2	13:57:49	14:01:16	0	90	3.27E-05	v. fine sand, clay laminate
17	0.15	11:17:18	11:17:27	0	90	5.63E-04	clean sands
18							
19	0.1	13:00:25	15:43:36	0	90	3.45E-07	v. fine sand, clay laminate
20	0.2	12:40:33	13:08:06	0	90	4.09E-06	v. fine sand, clay laminate
22	0.2	10:15:36	10:17:25	0	90	6.20E-05	v. fine sand, clay laminate
23	0.2	10:26:13	10:42:22	0	95	7.55E-06	v. fine sand, clay laminate
24	0.2	10:21:51	10:22:34	0	90	1.57E-04	clean sands
25	0.2	4:33:00	4:37:51	0	95	2.51E-05	v. fine sand, clay laminate
27							
28							
30	0.2	5:02:00	5:02:10	0	95	7.31E-04	clean sands
31	0.2	12:16:25	12:35:42	0	65	3.79E-06	v. fine sand, clay laminate
32							
33	0.2	11:14:35	11:22:30	0	90	1.42E-05	v. fine sand, clay laminate

Table 1 (cont.) Core permeabilities (*k*) by site indicating the permeability dependent sediment classification

site	core length (m)	initial time	final time	initial height (cm)	final height (cm)	k (m/s)	class
34	0.2	12:43:34	15:01:07	0	90	8.19E-07	v. fine sand, clay laminate
37	0.2	10:43:35	11:00:25	0	90	6.69E-06	v. fine sand, clay laminate
39	0.2	11:05:13	11:13:01	0	90	1.44E-05	v. fine sand, clay laminate
40	0.2	10:47:10	10:55:05	0	90	1.42E-05	v. fine sand, clay laminate
41	0.2	12:16:08	12:23:09	0	90	1.61E-05	v. fine sand, clay laminate
42	0.2	14:10:34	14:12:36	0	90	5.54E-05	v. fine sand, clay laminate
43	0.2	12:03:08	12:03:15	0	90	9.66E-04	clean sands
44	0.2	14:20:52	15:06:04	0	90	2.49E-06	v. fine sand, clay laminate
45	0.2	11:02:01	11:10:45	0	90	1.29E-05	v. fine sand, clay laminate
46	0.2	11:16:48	11:25:43	0	90	1.26E-05	v. fine sand, clay laminate
47	0.2	14:13:45	14:19:12	0	90	2.07E-05	v. fine sand, clay laminate
49	0.2	11:54:25	12:08:40	0	80	6.71E-06	v. fine sand, clay laminate
50	0.18	14:26:44	14:29:04	0	90	4.35E-05	v. fine sand, clay laminate
51	0.2	14:20:44	14:22:52	0	90	5.28E-05	v. fine sand, clay laminate
52	0.2	14:03:18	14:40:15	0	85	2.81E-06	v. fine sand, clay laminate
53	0.2	14:30:07	14:39:53	0	90	1.15E-05	v. fine sand, clay laminate
54	0.15	14:32:40	14:34:21	0	90	5.02E-05	v. fine sand, clay laminate
55	0.2	12:38:48	12:55:22	0	90	6.80E-06	v. fine sand, clay laminate
56	0.2	15:01:27	15:25:29	0	70	3.34E-06	v. fine sand, clay laminate
57	0.13	10:21:21	10:29:24	0	90	9.10E-06	v. fine sand, clay laminate
58	0.13	15:27:15	15:36:03	0	90	8.32E-06	v. fine sand, clay laminate
59	0.2	13:50:15	13:52:47	0	90	4.45E-05	v. fine sand, clay laminate
60	0.17	14:47:15	14:49:05	0	90	5.22E-05	v. fine sand, clay laminate
61	0.2	13:48:23	14:06:15	0	90	6.31E-06	v. fine sand, clay laminate
62	0.11	15:07:58	15:10:31	0	90	2.43E-05	v. fine sand, clay laminate
63	0.2	14:19:43	15:12:50	0	60	1.24E-06	v. fine sand, clay laminate
64	0.11	15:30:41	15:35:31	0	90	1.28E-05	v. fine sand, clay laminate
65	0.2	10:08:37	11:31:30	0	25	2.95E-07	v. fine sand, clay laminate
66	0.2	14:14:43	14:34:56	0	90	5.57E-06	v. fine sand, clay laminate
67	0.2	10:58:44	11:01:38	0	95	4.20E-05	v. fine sand, clay laminate
68	0.2	10:22:40	10:42:20	0	65	3.71E-06	v. fine sand, clay laminate
69	0.2	11:08:50	11:10:53	0	95	5.95E-05	v. fine sand, clay laminate
70	0.14	14:31:03	14:33:15	0	90	3.58E-05	v. fine sand, clay laminate
71	0.2	12:42:59	12:44:25	0	90	7.86E-05	v. fine sand, clay laminate
71	0.2	11:13:30	11:14:07	0	90	1.83E-04	clean sands
74	0.2	12:10:59	12:18:29	0	90	1.50E-05	v. fine sand, clay laminate
75	0.16	10:25:35	10:46:59	0	90	4.21E-06	v. fine sand, clay laminate
76	0.2	15:32:12	15:40:05	0	90	1.43E-05	v. fine sand, clay laminate
77	0.2	11:00:24	11:00:44	0	90	3.38E-04	clean sands
79	0.2	11:27:11	11:28:07	0	90	1.21E-04	clean sands
80	0.18	11:20:31	11:36:23	0	90	6.39E-06	v. fine sand, clay laminate
84	0.2	12:06:28	13:45:06	0	90	1.14E-06	v. fine sand, clay laminate
90	0.2	14:24:25	14:24:59	0	90	1.99E-04	clean sands
91	0.2	14:29:00	14:29:10	0	90	6.76E-04	clean sands
92	0.2	14:17:11	14:17:37	0	90	2.60E-04	clean sands
93	0.08	14:08:23	14:08:26	0	90	9.01E-04	clean sands
95	0.18	12:00:19	12:01:31	0	90	8.45E-05	v. fine sand, clay laminate
97	0.2	15:12:10	15:51:08	0	90	2.89E-06	v. fine sand, clay laminate
98	0.2	10:06:00	10:25:45	0	95	6.17E-06	v. fine sand, clay laminate
100	0.2	13:20:28	13:44:39	0	75	3.63E-06	v. fine sand, clay laminate
103	0.2	14:26:55	14:28:09	0	90	9.14E-05	v. fine sand, clay laminate
105	0.19	14:20:44	14:21:20	0	90	1.78E-04	clean sands
106	0.06	10:33:23	10:47:57	0	85	2.14E-06	v. fine sand, clay laminate
107	0.2	11:03:28	12:20:00	0	80	1.25E-06	v. fine sand, clay laminate

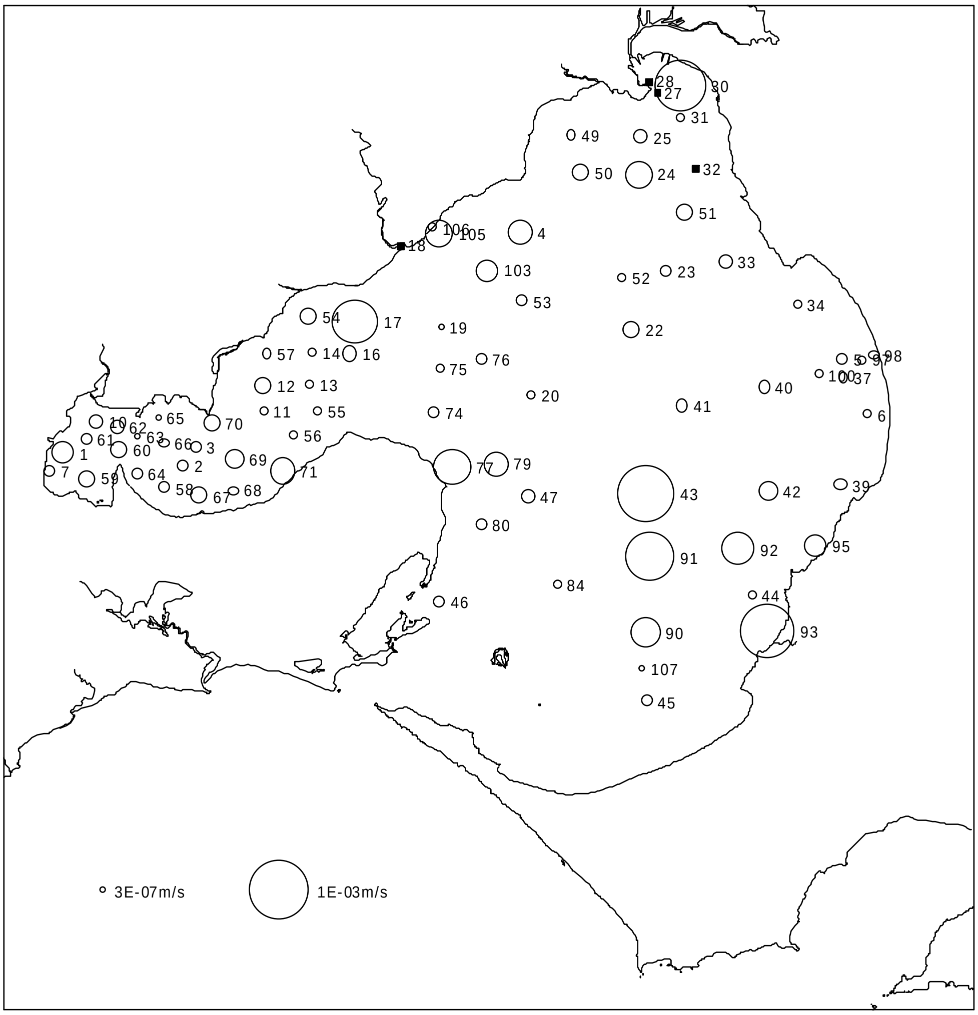

Figure 3: Permeability constants (*k*) at sampling sites (site numbers shown). The area of the circles are proportional to the magnitude of k. Dark squares represent sites where no data was obtained.

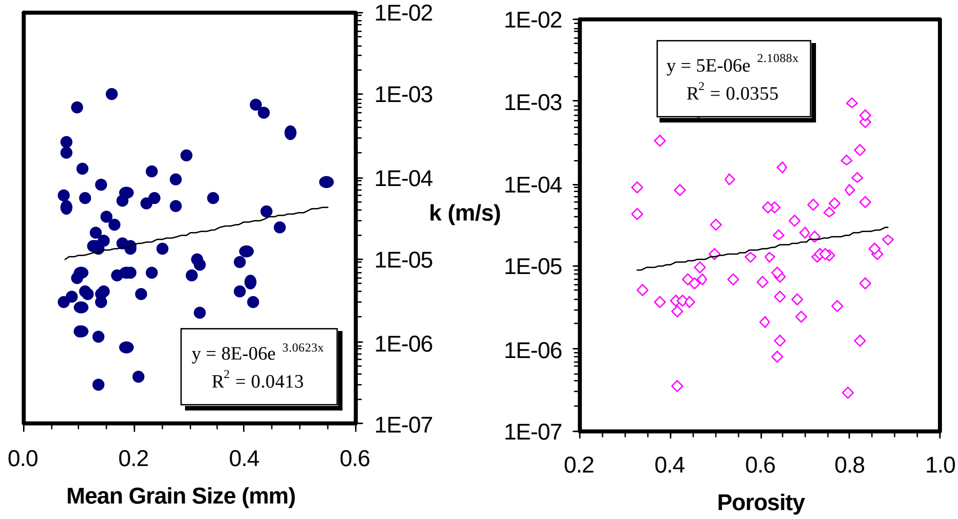

Figure 4: Variations of permeability *k* with grain size and porosity.

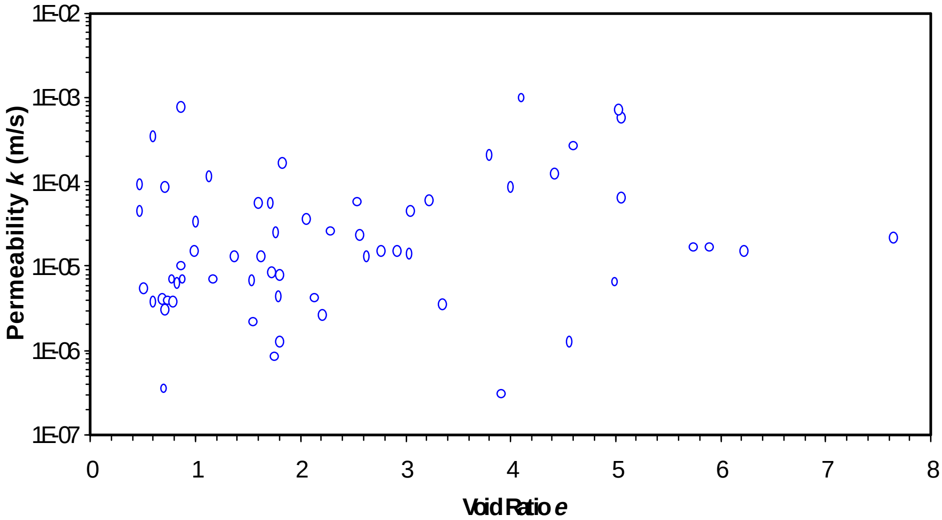

Figure 5: Relationship between permeability *k* and void ratio *e* measured in Port Phillip Bay.

3.2. Consolidation

Measurements of consolidation rates with time of sediments from 72 sites around Port Phillip Bay are shown in Table 2. An example of how the level of water-sediment interface varies with time is shown in Figure 6. It can be seen that the water-sediment interface falls with time in a manner similar to that observed by Berlamont *et al.* (1992).

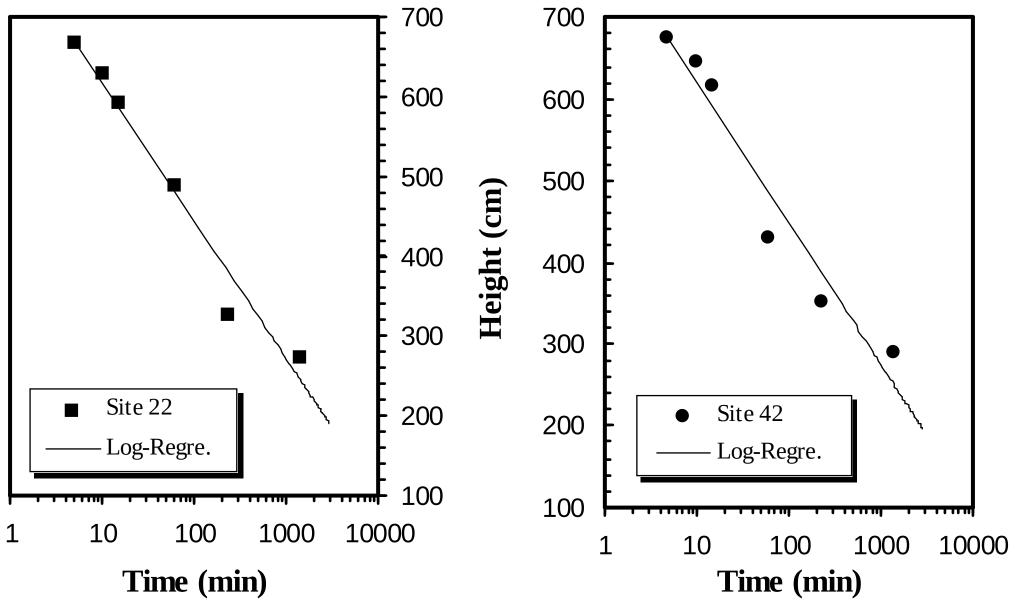

Figure 6: Variation of the level of the water-sediment interface with time measured from the samples collected at sites 22 and 42.

Care has to be taken as the result of the tests are very much influenced by the sample treatment and by the actual test conditions, such as filling techniques and the salinity of the pore water and the water into which it is poured. Low temperature in the laboratory is preferable as it reduces the production of organic matter which can have an influence on consolidation.

Table 2:Height of the sediment/water interface as the core consolidates over time.

site	Height (mm) at specified time (min)							
	0	5	10	15	60	240	1440	2880
1	700	682	671	660	563	414	357	
2	712	701	690	680	590	480	406	
3	705	700	690	675	565	501	429	
4	695	670	644	618	520	475	446	
5	695	670	645	620	521	476	448	
6	695	625	565	517	430	398	380	
7	695	679	668	657	560	413	352	
10	700	678	657	640	489	392	345	340
11	710	683	670	655	483	391	352	
12	700	673	654	631	482	430	400	
13	692	621	565	520	430	399	386	
14	690	650	616	582	459	422	407	
16	710	560	463	429	382	366	359	
17	698	432	409	400	375	367	362	
18								
19	640	490	404	389	365	357	354	
20	709	661	619	579	378	310	271	
22	700	668	629	591	490	326	274	
23	710	691	677	660	504	438	373	
24	700	694	679		540	548	382	
25	710	690	678	665	522	442	392	
27								
28								
30	700	420	405	400	389	382	386	
31	680	640	598		471	435	415	
32								
33	692	680	665	650	523	400	335	
34	700	690	679	667	556	487	446	
37	700	680	663	643	533	488	450	
39	695	670	645	620	487	448	418	415
40	692	682	661	639	495	425	358	
41	700	686	650	618	460	395	339	
42	700	676	646	617	427	350	289	
43	710	674	630	590	405	240	290	280
44	705	668	640	610	412	340	302	
45	690	660	636	608	482	431	402	400
46	690	363	349	349	349	350	350	350
47								
49	680	641	608	572	475	440	424	
50	700	649	596		417	366	335	
51	702	682	670	659	500	416	360	
52	700	694	680	669	577	455	398	
53								
54	698	373	365	362	357	354	352	
55	690	661	639	612	515	469	440	
56	700	688	674	665	562	452	410	
57	700	646	600	560	420	379	353	
58	690	677	679	559	562	461	420	
59	695	679	669	660	571	439	387	
60	683	390	392	389	380	379	377	
61	698	403	400	399	391	387	383	
62	705	682	661	640	507	450	418	
63	722	704	696	686	585	457	389	
64	695	683	679	680	610	568	400	
65	691	674	660	648	510	391	332	
66	695	682	667	653	530	411	363	
67	698	670	652	635	482	364	319	
68	708	680	660	639	474	393	350	
69	695	671	653	637	492	370	316	
70	695	613	553	515	459	435	426	

Table 2 (cont.) :Height of the sediment/water interface as the core consolidates over time.

site	Height (mm) at specified time (min)							
	0	5	10	15	60	240	1440	2880
71	680	576	510	472	422	408	400	
74	700	677	660	641	492	420	378	
75	700	669	647	622	448	384	342	
76	700	671	649	625	460	400	358	
77	700	267	268	268	268	269	268	268
79	705	664	630	597	391	319	270	212
80	690	649	614	578	427	370	342	
84	702	683	671	655	533	478	444	440
90	695	660	632	605	401	320	270	
91	705	680	645	613	427	354	297	
92	705	669	635	601	402	332	286	
93	700	320	326	326	326	322	320	
95	695	568	488	452	405	387	376	
97	698	560	475	450	410	390	385	
98	690	387	387	388	389	390	389	
100	700	685	674	663	555	452	397	
103								
105								
106	705	690	683	677	595	492	449	
107	690	680	661	650	510	443	404	

3.3. Viscosity

Flow and viscosity curves for each sample run are held at MAFRI. Figure 7 shows flow and viscosity curves for site 47 which is typical of those measured at the 46 sites for which viscosity measurements were made.

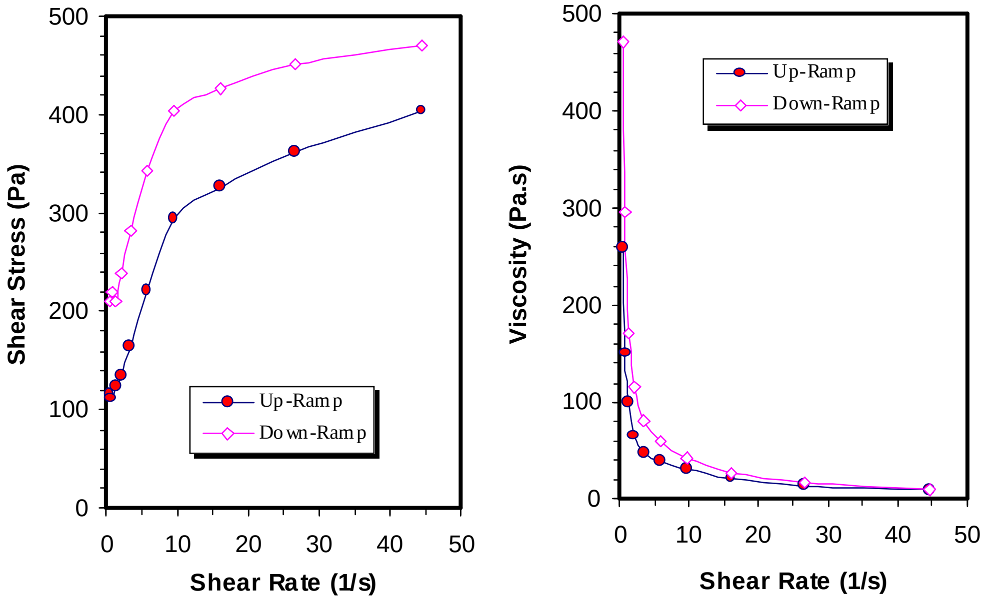

Figure 7: The rheological behaviour of sediment at site 47.

It can be seen that the up-ramp curves lie below the down-ramp curves. This is opposite to what former investigators have found [e.g. Migniot (1968), Migniot and Hamm (1990)].

The collected samples may contain two components; one is the *thixotropic* substance and the other is the *rheopective* substance. The thixotropic substances display an additional characteristic that affects their behaviour under shear stress. These substances display internal bonding to result in a 3-dimensional intermolecular network of bonds. Their natural (non-sheared) state is called a *gel*. The application of shear stress not only aligns the particles or molecules, but also breaks down the intermolecular bonds at sufficiently high shear rates. In this highly sheared state, the substance is termed a *sol*. Once the shear force is removed, the inter-molecular bonding will in time be re-established. The transition from gel to sol and from sol to gel is reproducible many times. True thixotropic substances will plot up-ramps above down-ramps on a flow curve. However, the rheopective substances show viscosity opposite trends to the thixotropic substances, that is an increase in shear rate will result in an increase in viscosity. This implies that the up-ramps will lie below the down-ramps on the flow-viscosity curves. On the basis of this, the sediments in Port Phillip Bay may be classified as rheopective substances.

An explanation for this probably lies in the fact that the majority of Port Phillip Bay sediments are fine sand with little or no clay content so that settling of sand particles may occur during the time of down-ramps (angular speed reducing). Hence the cohesiveness of sediments or the bonding between flocs or individual particles becomes stronger since the sediment cohesion increases with decreasing sand content in the sample.

The authors believe that the up-ramp curves are of most significant since they give the best information concerning the initial entrainment of sediment by fluid flow.

For engineering purposes, efforts are usually concentrated on the determination of the Bingham parameters, those being the yield stress τ_y, the Bingham stress τ_B, and the viscosity constant μ_∞.

The measurement of the yield stress τ_y has received much attention because the critical shear stress for erosion is expected to have a correlation with τ_y as shown by Otsubo and Muraoka (1988).

There are two critical shear stresses τ_{c1} and τ_{c2} used for the threshold in mud transport. The stress τ_{c1} is the threshold where mud particles begin to be dislodged as the shear stress under which the amount of dislodged mud particles exceeded 3.5×10^{-5} kg/m^2/s. This is similar to the threshold for sand particles as defined by Otsubo and Muraoka (1988). On the other hand, the τ_{c2} threshold is where the bottom bed begins to be destroyed by currents, and a great deal of mud is swept away. According to this definition, τ_{c1} is smaller than τ_{c2}.

It was experimentally found by Otsubo and Muraoka (1989) that the two critical shear stresses τ_{c1} and τ_{c2} had good correlation with the yield stress τ_y, which were expressed as

$$\tau_{c1} = 0.27\,\tau_y^{0.6} \qquad \text{Equation 1}$$

$$\tau_{c2} = 0.79\,\tau_y^{0.94} \qquad \text{Equation 2}$$

Since the yield stress τ_y measured at 42 sites around Port Phillip Bay ranges from 7.0 to 400 Pa as shown in Figure 8, the two critical shear stresses calculated from Equations 1 and 2 are:

$$\tau_{c1} = 0.86 \sim 9.83\text{Pa} \qquad \text{Equation 3}$$

$$\tau_{c2} = 4.92 \sim 220\text{Pa} \qquad \text{Equation 4}$$

Correspondingly, the minimum shear velocity required from currents and waves to initiate movement of sediment particles is:

$$u^*_{c1} = \sqrt{\frac{\tau_{c1}}{\rho_w}} = 0.03 \sim 0.31\text{m/s} \qquad \text{Equation 5}$$

and the minimum shear velocity required from currents and waves to destroy the consolidated bed and stir up mud into suspension is

$$u^*_{c2} = \sqrt{\frac{\tau_{c2}}{\rho_w}} = 0.07 \sim 0.47\text{m/s} \qquad \text{Equation 6}$$

As seen from Equations 3 and 4, the critical shear stresses vary significantly from place to place and, thus, a universal constant value for τ_{c1} or τ_{c2} may not be applicable in Port Phillip Bay.

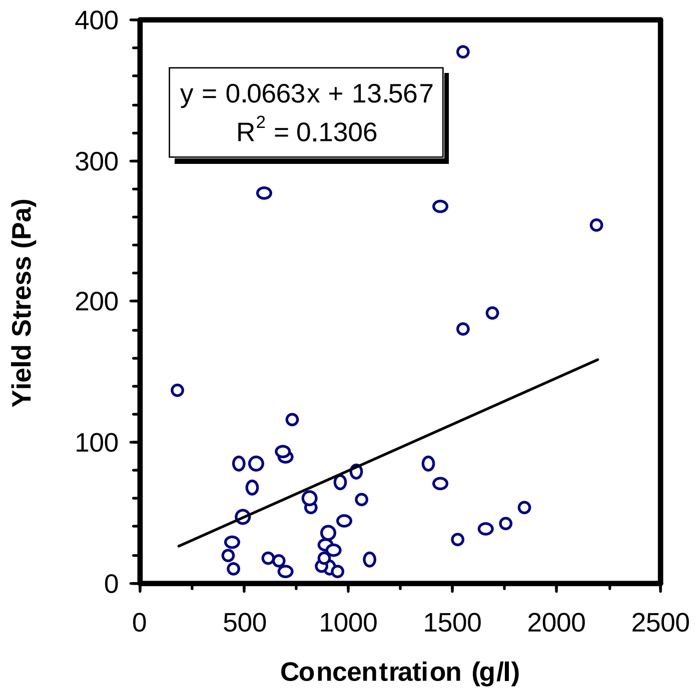

Figure 8: Yield stresses estimated from flow curves measured at 42 sites.
The range of the yield stress τ_y is from 7.0 to 400 Pa and the concentration of collected samples varies from 189 to 2200 g/L.

3.4. Settling Velocity and Grain Size Distributions

Measurements of grain size and settling velocity distributions for each collected sample are held at MAFRI. A statistical summary of the grain size distributions is given in Table 3, and of the textural descriptions in Table 4.

The settling velocity distributions at sites 80 and 84 (Figure 9) are typical of Port Phillip Bay. The notation used is as follows:

Δw_i = the interval weight for the *i*th group of sediments

$\Sigma \Delta w_i$ = the total weight of sediment sample used

$\frac{\Delta w_i}{\sum \Delta w_i}$ = the interval frequency

Correspondingly, the grain size distribution at sites 80 and 84 can be calculated from measured settling velocities in Figure 9 using the Gibbs equation (Gibbs *et al* 1971), and are shown in Figure 10. Consequently, the calculated grain size distribution would primarily depend on how accurately the settling velocities are measured in a settling tube, but also on the assumptions made in applying the Gibbs equation.

The design of the settling tube system and the procedures adopted in using it, as discussed in Section 2.5, address the problems of wall effects and clumping of sediment. The latter is most likely to affect measurements in the small tube, and for some cohesive samples clumps of sediment could be observed falling out rapidly, reaching the collecting plate without breaking up. In merging results from the two fall tubes, however, high fall velocity data are taken from the large tube so the combined spectrum should not be affected.

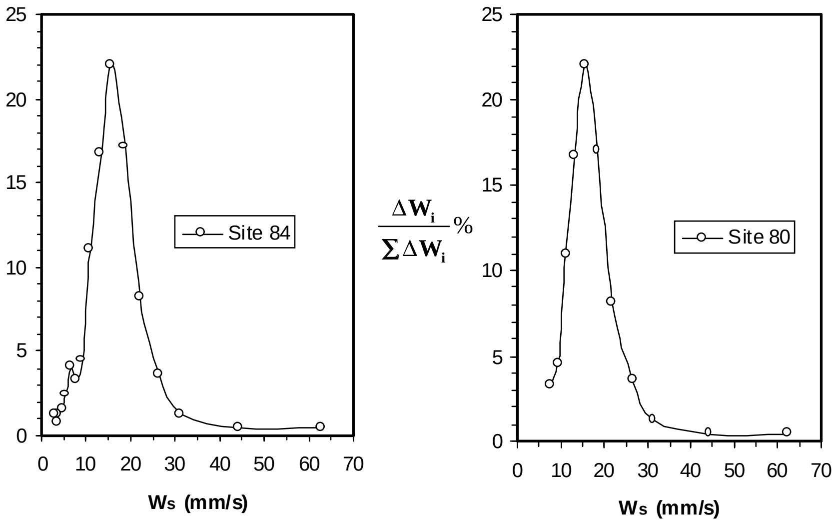

Figure 9: Settling velocity distributions at sites 80 and 84.
The median settling velocities are 10.2 and 17.5 mm s^{-1} respectively.

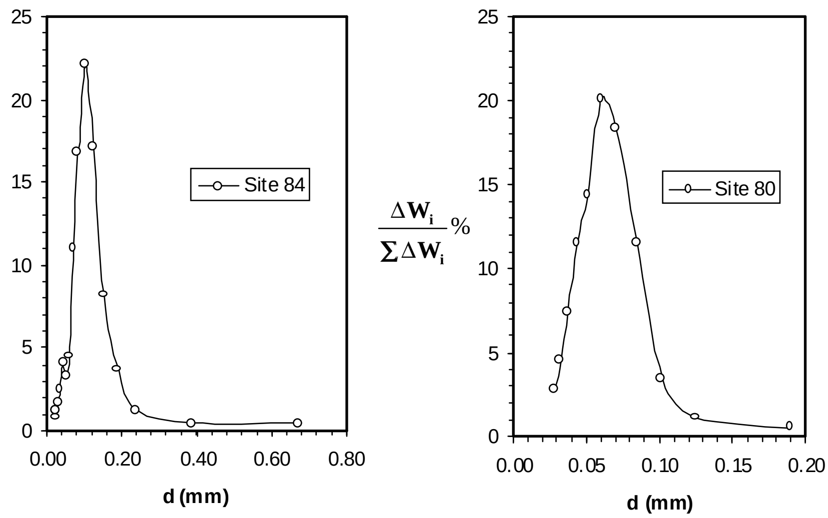

Figure 10: Grain size distributions at sites 80 and 84.
The median grain sizes are 0.12 and 0.17 mm respectively.

It should be mentioned here that grain sizes calculated from the Gibbs equation are standardised to an equivalent quartz-density grain, using a constant grain density (ρ_s = 2650 kg/m$^{3)}$ for all samples collected at the 80 sites. Because of the variation of sediment density between samples, these may differ significantly from the actual grain sizes. Figure 11 shows an example of how the grain size varies with the relative density s (=ρ_s / ρ_w) at a given settling velocity w_{ss}, where the error percentage is defined as

$$\textbf{Error} = \frac{|d(\mathrm{s}) - d(2.65)|}{d(\mathrm{s})} \times 100\% \qquad \text{Equation 7}$$

in which d(s) is the diameter of sediment assuming a relative density (s). It can be seen from Figure 11 that the actual grain size calculated by the Gibbs equation with the relative density less than (or more than) 2.65 is underestimated (or overestimated) if the relative density is chosen to be a constant 2.65, and that the percentage error estimated from Equation 7 can be significant for realistic relative densities.

The distribution of median grain size in Port Phillip Bay, shown qualitatively in Figure 12, is consistent with that of Beasley (1966). A corresponding plot of the silt-clay fraction as a percentage of the total sample at each site is shown in Figure 13. The two quantities are inversely related; the larger the silt-clay fraction, the smaller the median grain size. Larger grain sizes are generally evident at nearshore sites, while fine muds are found at deeper sites in the Central Bay and the Geelong Arm.

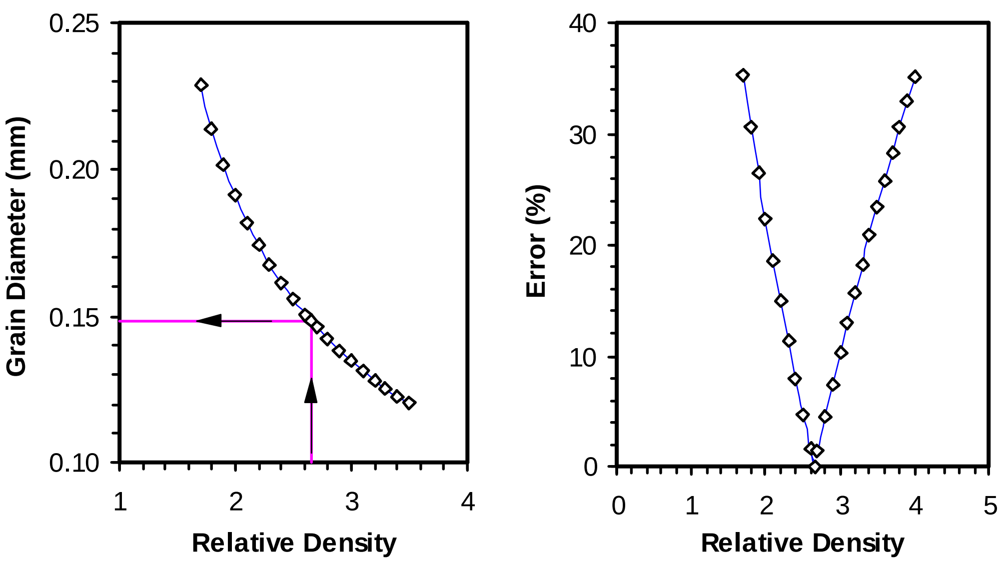

Figure 11: Variation of grain sizes with actual relative density ρ_s / ρ_w calculated from the Gibbs equation using a nominal relative density of 2.65. The settling velocity w_s is taken as 1.5 cm/s.

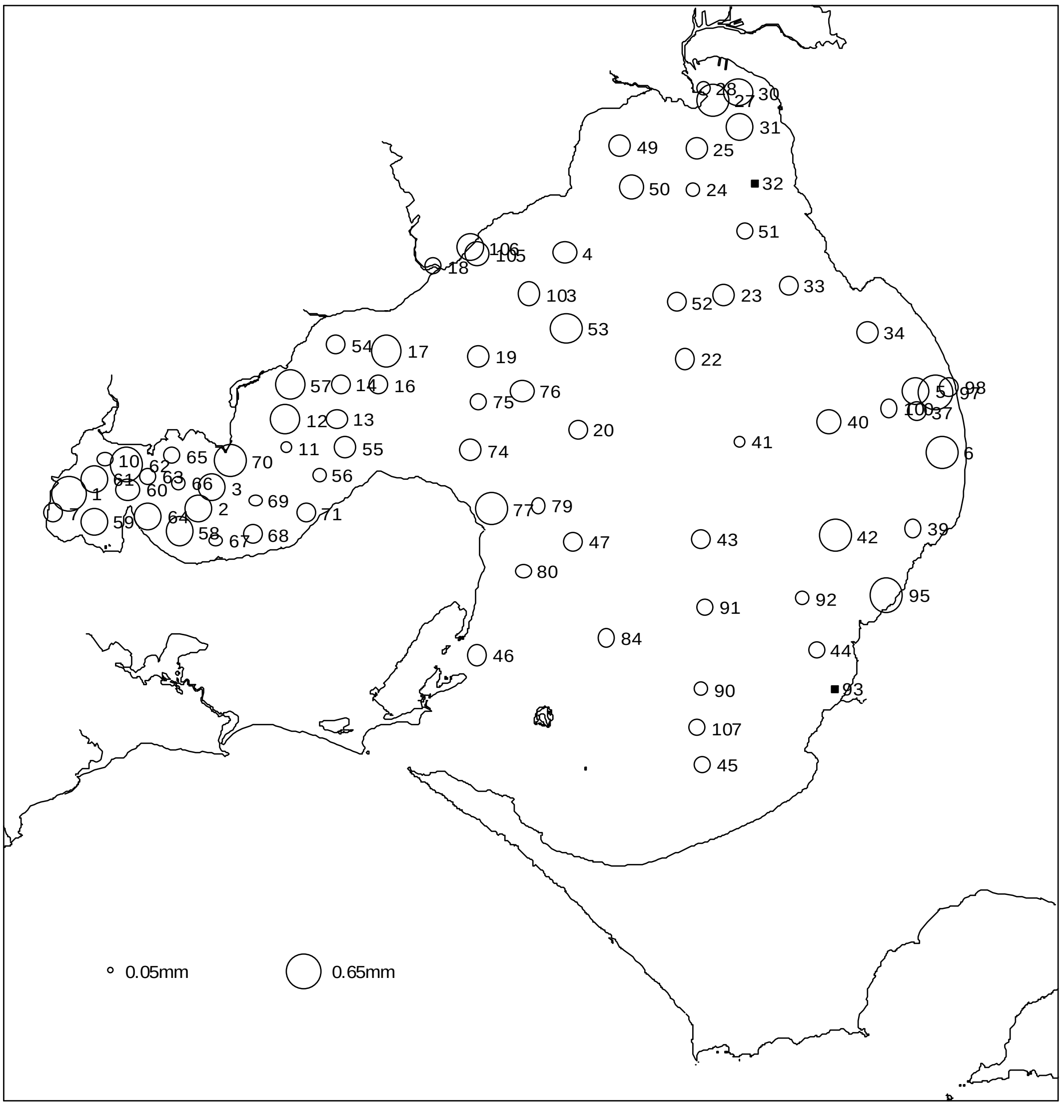

Figure 12: Median grain sizes (mm) at sampling sites (site numbers shown). The area of the circles are proportional to grain size. Dark squares denote sites where no data was obtained.

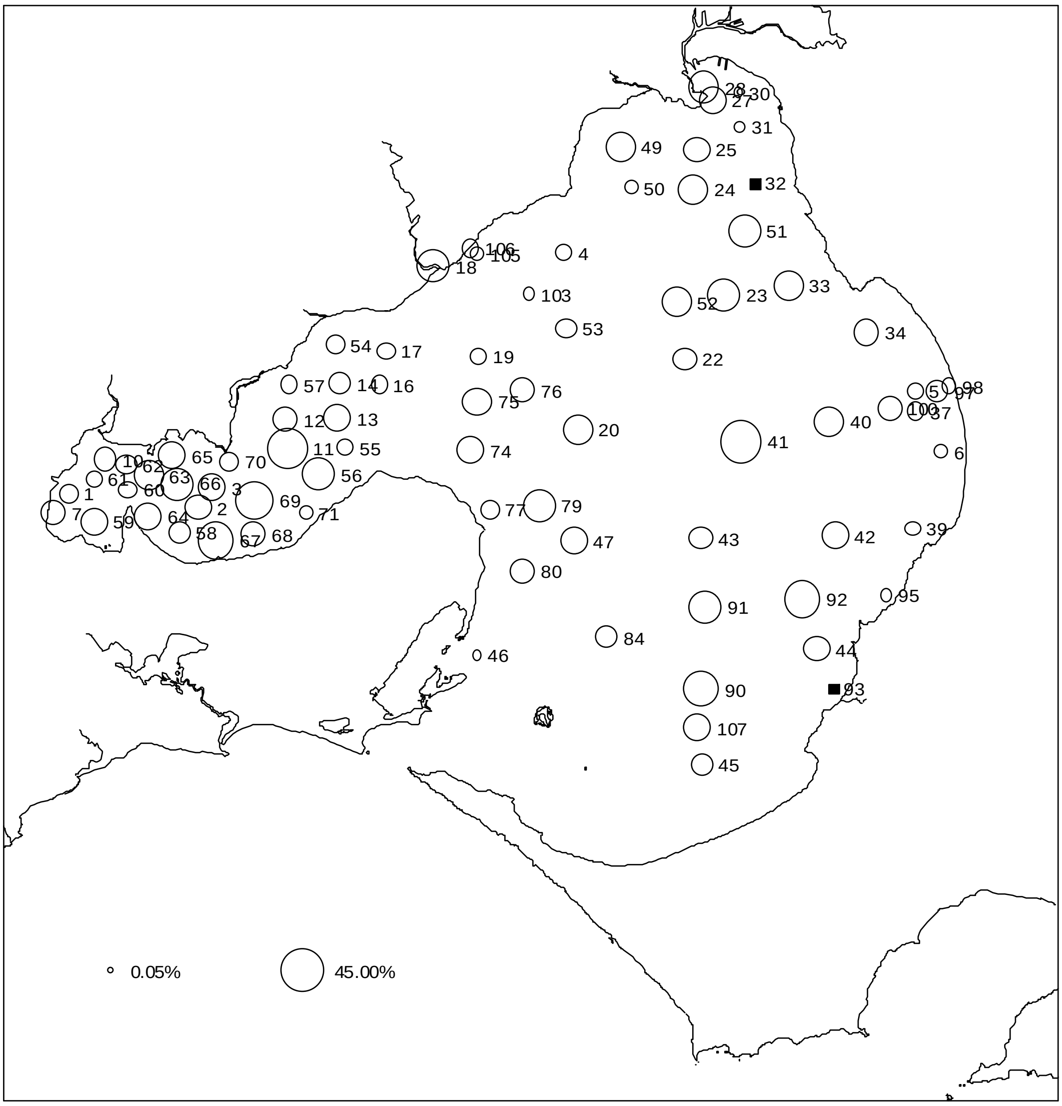

Figure 13: Silt and clay fraction as a percentage of total at sampling sites (site numbers shown). The area of the circles is proportional to % fraction. Dark squares denote sites where no data was obtained.

Table 3: Summary of grain size analysis statistics.

site	mean (f)	sorting (f)	skewness	kurtosis	median (f)	median (mm)
1	1.31	1.40	2.32	5.78	0.75	0.60
2	1.80	1.68	1.49	1.49	1.27	0.41
3	2.21	1.69	1.06	0.18	1.44	0.37
4	2.08	1.00	1.44	4.63	1.96	0.26
5	1.66	1.22	1.86	5.93	1.37	0.39
6	1.27	1.23	1.51	3.95	0.95	0.52
7	2.76	1.14	1.88	4.15	2.41	0.19
10	3.35	0.85	1.02	4.52	3.35	0.10
11	3.76	1.16	0.26	1.25	3.78	0.07
12	1.54	1.57	1.63	2.35	1.17	0.44
13	2.21	1.43	0.12	-1.27	2.50	0.18
14	2.77	0.95	1.43	4.14	2.62	0.16
16	2.69	0.73	1.29	6.13	2.62	0.16
17	1.19	1.20	2.79	10.01	0.98	0.51
18	3.12	1.53	0.63	0.15	2.83	0.41
19	2.25	0.94	1.14	4.72	2.24	0.21
20	3.15	1.36	1.09	0.95	2.82	0.14
22	2.40	1.30	0.67	0.93	2.30	0.20
23	2.94	1.81	0.93	-0.31	2.19	0.22
24	3.60	0.94	1.80	3.93	3.38	0.10
25	2.60	1.30	1.45	2.47	2.25	0.21
27	1.53	1.78	1.15	0.71	1.06	0.48
28	3.88	0.86	1.97	3.43	3.52	0.09
30	1.24	0.58	5.12	52.52	1.26	0.42
31	1.35	0.74	2.68	15.11	1.29	0.41
32						
33	2.95	1.21	0.86	0.60	2.68	0.16
34	2.41	1.51	0.87	0.61	2.16	0.22
37	2.36	1.15	1.11	4.32	2.39	0.19
39	2.90	0.66	2.75	21.39	2.83	0.14
40	2.48	1.85	1.32	0.81	1.72	0.30
41	4.05	1.28	0.51	0.11	3.81	0.07
42	1.91	1.95	1.63	1.49	0.97	0.51
43	2.65	1.08	1.24	2.86	2.45	0.18
44	3.22	0.96	1.52	4.12	3.07	0.12
45	2.86	0.93	2.29	7.78	2.66	0.16
46	2.35	0.48	-1.13	45.99	2.33	0.20
47	2.90	1.15	1.31	1.89	2.57	0.17
49	2.41	1.86	0.69	-0.05	2.06	0.24
50	1.85	0.89	2.69	12.56	1.71	0.30
51	3.15	1.36	0.30	0.56	2.97	0.13
52	2.84	1.55	0.96	0.31	2.44	0.18
53	1.30	1.35	1.89	4.08	1.02	0.49
54	2.45	0.96	0.05	4.81	2.40	0.19
55	2.08	1.10	1.64	6.93	2.09	0.23
56	3.47	1.06	1.17	1.62	3.31	0.10
57	1.35	1.32	1.51	3.11	1.12	0.46
58	1.65	1.31	2.00	4.99	1.36	0.39
59	2.13	1.73	0.73	-0.38	1.51	0.35
60	2.07	1.28	2.74	9.69	1.89	0.27
61	1.71	0.97	2.13	8.80	1.68	0.31
62	1.10	1.36	2.58	6.42	0.77	0.59
63	3.23	1.11	1.11	1.54	3.00	0.12
64	1.99	1.72	0.78	-0.05	1.56	0.34
65	2.86	1.39	0.40	0.34	2.79	0.14
66	3.35	1.28	0.73	1.07	3.16	0.11
67	3.69	1.26	0.65	0.73	3.49	0.09
68	2.84	1.22	0.94	1.80	2.72	0.15
69	3.73	1.23	0.55	0.61	3.52	0.09
70	1.18	1.31	2.52	7.39	0.87	0.55
71	2.78	0.61	3.12	23.13	2.75	0.15
74	2.46	1.46	0.80	0.69	2.23	0.21
75	3.04	1.25	1.09	1.27	2.79	0.14
76	2.37	1.29	1.17	1.77	2.03	0.25
77	1.04	1.34	2.98	11.63	0.91	0.53
79	3.17	1.27	0.09	0.03	3.18	0.11

Table 3 (cont.): Summary of grain size analysis statistics.

site	mean (f)	sorting (f)	skewness	kurtosis	median (f)	median (mm)
80	3.24	0.86	2.29	8.61	3.02	0.12
84	2.84	0.98	2.38	6.66	2.57	0.17
90	3.70	1.13	1.01	1.88	3.50	0.09
91	3.30	1.48	0.91	0.81	2.94	0.13
92	3.65	1.14	0.70	0.92	3.50	0.09
93						
95	0.86	0.78	4.97	32.63	0.75	0.60
97	1.26	1.71	1.91	2.99	0.62	0.65
98	2.56	1.00	2.21	12.12	2.47	0.18
100	3.06	1.04	1.23	2.66	2.92	0.13
103	1.85	0.72	1.63	10.07	1.85	0.28
105	1.74	0.92	1.76	5.38	1.55	0.34
106	1.64	1.31	1.17	2.23	1.52	0.35
107	3.28	1.05	1.11	3.40	3.09	0.12

Table 4: Sediment textural compositions.

site	gravel	sand	silt	clay
1	0.00%	93.96%	5.60%	0.44%
2	0.00%	87.71%	12.29%	0.00%
3	0.00%	83.14%	16.86%	0.00%
4	0.00%	96.03%	3.94%	0.03%
5	0.00%	96.73%	2.96%	0.31%
6	0.18%	97.54%	2.23%	0.05%
7	0.00%	87.78%	11.85%	0.37%
10	0.00%	89.33%	10.67%	0.00%
11	0.00%	59.15%	40.57%	0.28%
12	0.00%	87.85%	11.91%	0.24%
13	0.11%	84.14%	15.75%	0.00%
14	0.00%	91.57%	8.34%	0.09%
16	0.00%	95.69%	4.28%	0.03%
17	0.00%	95.32%	4.68%	0.00%
18	0.00%	75.33%	24.39%	0.28%
19	0.00%	96.03%	3.89%	0.08%
20	0.00%	80.20%	19.80%	0.00%
22	0.00%	90.30%	9.70%	0.00%
23	0.00%	73.89%	26.11%	0.00%
24	0.00%	79.85%	19.86%	0.29%
25	0.00%	87.02%	12.64%	0.34%
27	0.63%	85.61%	13.37%	0.39%
28	0.00%	78.65%	21.35%	0.00%
30	0.00%	99.27%	0.66%	0.07%
31	0.00%	98.93%	1.07%	0.00%
32				
33	0.00%	81.42%	18.58%	0.00%
34	0.00%	86.54%	13.42%	0.04%
37	0.00%	95.73%	4.09%	0.18%
39	0.00%	97.14%	2.79%	0.07%
40	0.00%	81.34%	17.84%	0.82%
41	0.00%	55.99%	44.01%	0.00%
42	0.00%	84.62%	14.56%	0.82%
43	0.00%	90.41%	9.59%	0.00%
44	0.00%	86.66%	13.09%	0.25%
45	0.00%	92.15%	7.68%	0.17%
46	0.41%	99.11%	0.47%	0.01%
47	0.00%	85.26%	14.74%	0.00%
49	0.00%	79.95%	20.05%	0.00%
50	0.00%	97.65%	2.30%	0.05%
51	0.00%	76.06%	23.63%	0.31%
52	0.00%	79.82%	20.18%	0.00%

Table 4 (cont.): Sediment textural compositions.

site	gravel	sand	silt	clay
53	0.00%	93.66%	6.29%	0.05%
54	0.67%	94.96%	4.37%	0.00%
55	0.00%	95.93%	3.80%	0.27%
56	0.00%	76.24%	23.76%	0.00%
57	0.14%	94.79%	4.94%	0.13%
58	0.00%	92.24%	7.47%	0.29%
59	0.21%	83.09%	16.54%	0.16%
60	0.00%	94.46%	4.61%	0.93%
61	0.00%	96.64%	3.36%	0.00%
62	0.00%	92.38%	7.62%	0.00%
63	0.00%	79.92%	20.08%	0.00%
64	0.16%	84.13%	15.64%	0.07%
65	0.00%	82.95%	17.05%	0.00%
66	0.00%	75.81%	23.87%	0.32%
67	0.00%	66.98%	32.69%	0.33%
68	0.00%	87.03%	12.83%	0.14%
69	0.00%	64.99%	35.01%	0.00%
70	0.00%	94.50%	5.33%	0.17%
71	0.00%	98.10%	1.80%	0.10%
74	0.00%	85.17%	14.64%	0.19%
75	0.00%	81.86%	18.04%	0.10%
76	0.00%	88.42%	11.45%	0.13%
77	0.78%	94.88%	3.84%	0.50%
79	0.00%	77.71%	22.29%	0.00%
80	0.00%	89.12%	10.68%	0.20%
84	0.00%	90.22%	9.63%	0.15%
90	0.00%	71.04%	28.85%	0.11%
91	0.00%	75.89%	23.50%	0.61%
92	0.00%	69.46%	30.54%	0.00%
93				
95	0.00%	98.61%	1.34%	0.05%
97	0.00%	90.48%	9.52%	0.00%
98	0.00%	97.22%	2.19%	0.59%
100	0.00%	87.44%	12.56%	0.00%
103	0.00%	98.77%	1.23%	0.00%
105	0.00%	97.11%	2.89%	0.00%
106	0.00%	94.44%	5.53%	0.03%
107	0.00%	83.56%	16.36%	0.08%

3.5. Sediment Density and Bulk Density

Sediment density ρ_s and bulk density ρ_b are directly measured and are considered as two constitutive parameters in the present study. Other parameters such as water content $W_{\%}$, porosity P and void ratio e can be calculated on the basis of ρ_s and ρ_b. The density of the pore water is taken as $\rho_w = 1025$ kg/m^3. The variation of ρ_s and ρ_b in the top layer (0 - 5 cm) of cores collected at 80 sites around Port Phillip Bay is shown in Figure 14, and the values found for the above parameters at each site are summarised in Table 5. It can be seen that the sediment density ρ_s varies between 1563 and 3239 kg/m^3 while the bulk density ρ_b ranges from 1103 to 2054 kg/m^3. The range of sediment densities found indicates that the use of a constant sediment density ρ_s in the Gibbs equation may cause a discrepancy between the measured grain size, which is standardised to a quartz density equivalent, and the actual grain sizes. The spatial distribution of sediment and bulk densities within the Bay is presented in

Figure 16. Low densities (both ρ_s and ρ_b) are notable at the Central Bay and the Geelong Arm sites where small grain sizes were found.

Figure 15 shows the variations of sediment density ρ_s and bulk density ρ_b with depth below the top of core collected at site 68. It shows that the sediment density ρ_s changes irregularly with depth and that the bulk density ρ_b increases slightly with depth.

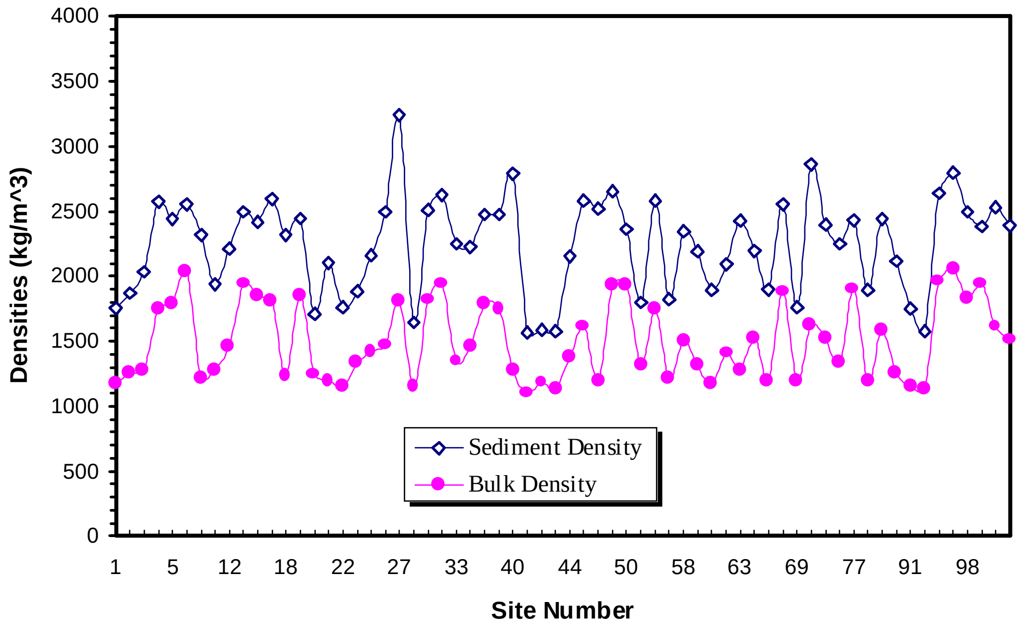

Figure 14: Variations of sediment density ρ_s and bulk density ρ_b measured in the top layer (2 cm thick) of core at each of the sample sites.

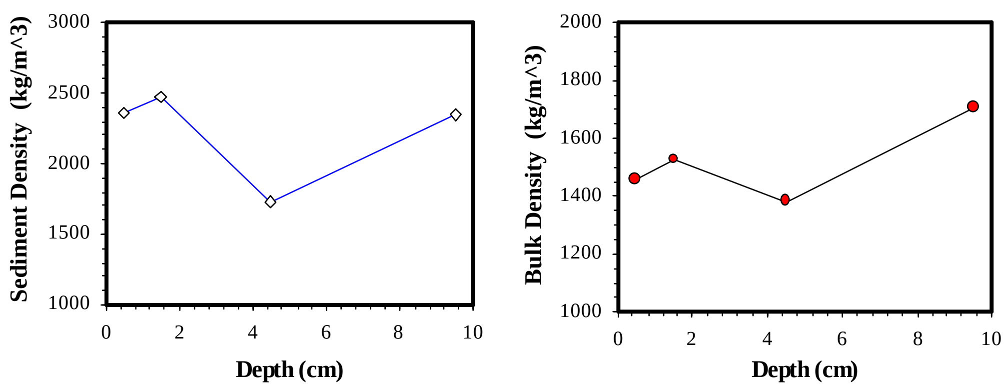

Figure 15: Variations of sediment density ρ_s and bulk density ρ_b measured with distance below the top of sample collected at site 68.

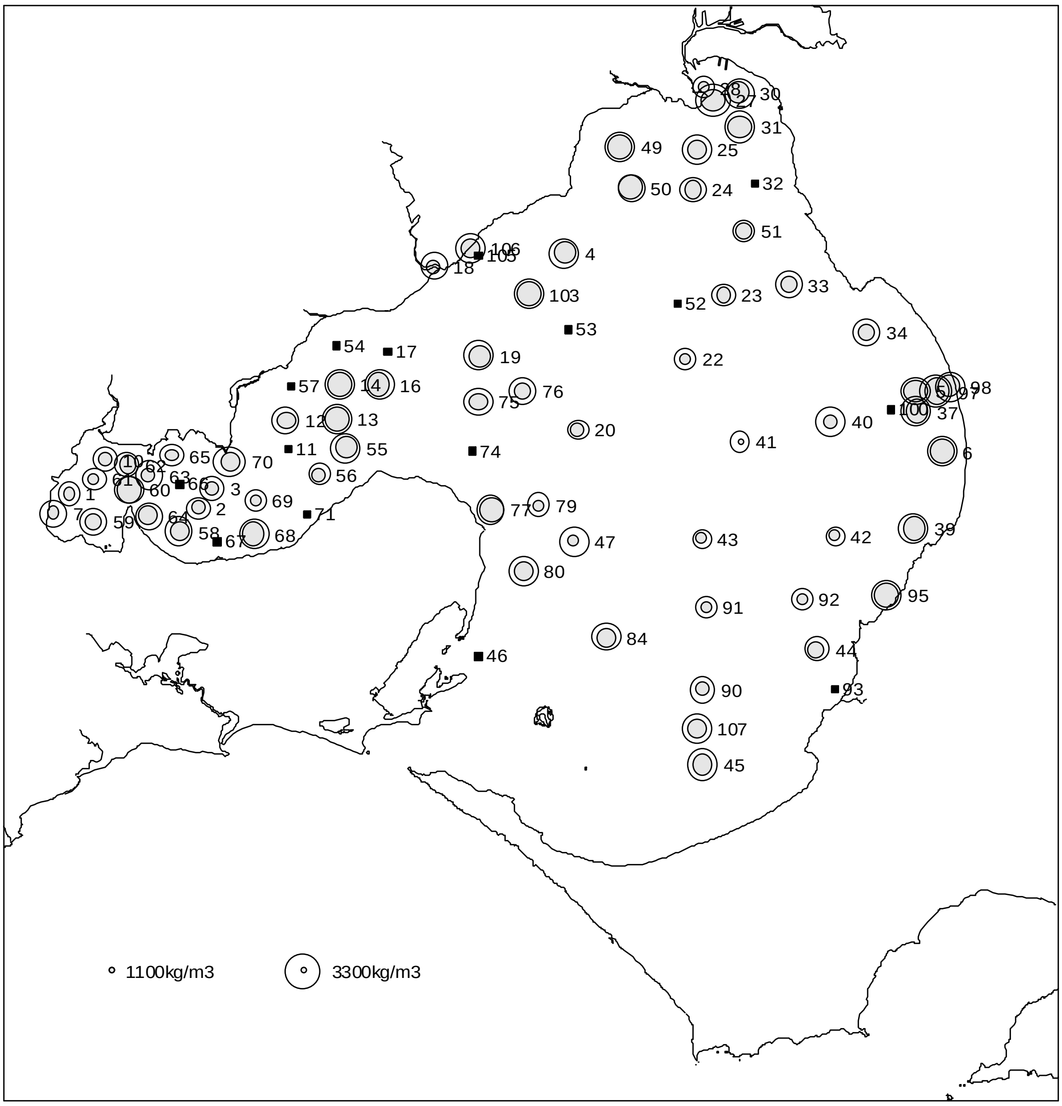

Figure 16: Sediment density and bulk density (shaded circles) at sampling sites (site numbers shown). The area of the circles is proportional to density. Dark squares denote sites where no data was obtained.

The void ratio *e* has been used as an important parameter in studying the consolidation of deposited sediments on the bed. In the consolidation theory, the effective stress σ´ and the permeability *k* are assumed to be the function of the void ratio *e*, that is σ´ = σ´(*e*) and *k* = *k*(*e*). Figure 17 shows the variation of void ratio *e* with different locations in Port Phillip Bay.

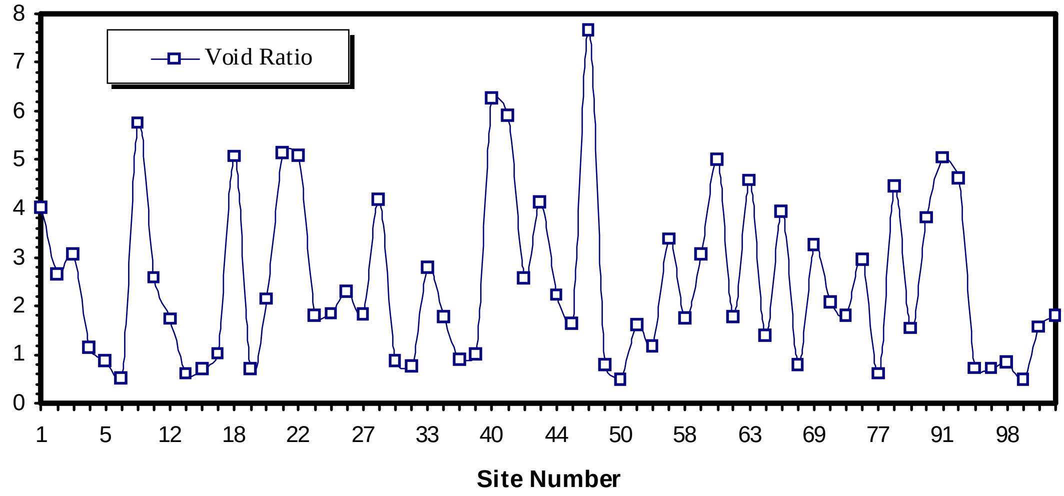

Figure 17: Variation of void ratio *e* measured in the top layer (2 cm thick) of core at each of the sample sites.

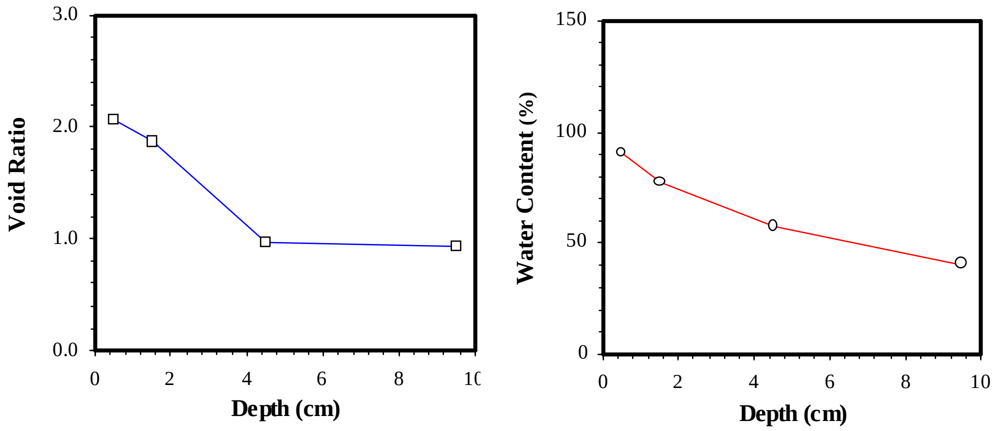

Figure 18: Variations of void ratio *e* and water content $W_{\%}$ with distance below the top of core collected at PPBES site 68.

It can be seen from Figure 17 that the void ratio *e* measured in the top layer of core samples varies significantly from 0.48 to 7.68. Higher void ratios are generally evident in deeper areas (central Port Phillip Bay) and areas near inputs of fine materials (Yarra River and Corio Bay).

The relationship between the void ratio *e* and the permeability *k* was addressed in more detail in Section 3.1.

Figure 18 shows the variation of the void ratio *e* and the water content $W_{\%}$ with distance from the top of core collected at site 68. It can be seen that the void ratio *e* and the water content $W_{\%}$ decrease with increasing depth.

Porosities measured in the Port Phillip Bay surface samples are somewhat larger than typical values, identified by Todd (1959), as 0.3-0.4 for sands, and up to 0.6 for silt, clay and mud. However, the results for site 68 suggest that porosities at deeper levels may be closer to this range.

Table 5: Summary of core density results.

site	Volume of core (m^3)	Mass of wet sample (kg)	Mass of dry sample (kg)	Particle density (kg/m^3)	Bulk density (kg/m^3)	Water content	Porosity	Void ratio
1	6.783E-05	0.079	0.024	1756	1171	234.0%	0.80	4.01
2	8.552E-05	0.108	0.044	1873	1258	144.5%	0.73	2.64
3	7.475E-05	0.095	0.038	2034	1275	153.3%	0.75	3.04
4	6.071E-05	0.106	0.073	2572	1747	45.5%	0.53	1.14
5	4.614E-05	0.082	0.060	2438	1781	36.5%	0.46	0.87
6	7.991E-05	0.163	0.135	2554	2034	20.7%	0.34	0.51
7	6.092E-05	0.074	0.021	2321	1217	253.8%	0.85	5.75
10	5.929E-05	0.076	0.032	1940	1280	136.6%	0.72	2.58
11								
12	9.655E-05	0.141	0.078	2213	1460	80.1%	0.63	1.73
13	9.260E-05	0.180	0.144	2499	1940	25.1%	0.38	0.61
14	8.755E-05	0.161	0.124	2419	1843	29.8%	0.41	0.70
16	9.214E-05	0.166	0.119	2597	1806	40.0%	0.50	1.01
17								
18	5.032E-05	0.062	0.019	2321	1239	223.6%	0.84	5.06
19	5.508E-05	0.102	0.079	2445	1856	29.8%	0.42	0.71
20	5.159E-05	0.064	0.028	1709	1243	128.4%	0.68	2.14
22	1.045E-04	0.120	0.030	1759	1146	295.5%	0.84	5.07
23	6.044E-05	0.080	0.041	1884	1331	98.3%	0.64	1.81
24	6.433E-05	0.092	0.049	2159	1424	87.4%	0.65	1.84
25	5.935E-05	0.087	0.045	2498	1472	94.2%	0.70	2.30
27	7.018E-05	0.127	0.080	3240	1808	57.9%	0.65	1.83
28	7.169E-05	0.082	0.023	1646	1145	260.2%	0.81	4.18
30	6.283E-05	0.114	0.084	2509	1820	35.4%	0.46	0.87
31	6.096E-05	0.118	0.092	2627	1941	29.3%	0.43	0.75
32								
33	7.480E-05	0.101	0.045	2247	1349	126.6%	0.74	2.78
34	7.703E-05	0.112	0.062	2228	1460	81.2%	0.64	1.77
37	7.459E-05	0.134	0.098	2476	1792	36.9%	0.47	0.89
39	7.059E-05	0.124	0.088	2476	1752	41.3%	0.50	1.00
40	6.283E-05	0.080	0.024	2792	1269	229.1%	0.86	6.24
41	7.155E-05	0.079	0.016	1564	1103	386.6%	0.86	5.90
42	5.541E-05	0.066	0.025	1586	1183	165.2%	0.72	2.56
43	7.654E-05	0.087	0.024	1578	1133	267.2%	0.80	4.11
44	8.759E-05	0.121	0.059	2157	1377	105.3%	0.69	2.22
45	5.952E-05	0.096	0.058	2581	1615	65.1%	0.62	1.64
46								
47	8.113E-05	0.097	0.024	2520	1198	311.4%	0.88	7.66
49	7.174E-05	0.139	0.107	2654	1937	30.4%	0.44	0.79
50	6.712E-05	0.129	0.107	2365	1927	21.1%	0.33	0.49

Table 5 (cont.): Summary of core density results.

site	Volume of core (m^3)	Mass of wet sample (kg)	Mass of dry sample (kg)	Particle density (kg/m^3)	Bulk density (kg/m^3)	Water content	Porosity	Void ratio
51	5.856E-05	0.077	0.040	1798	1322	91.6%	0.62	1.61
52								
53								
54								
55	7.439E-05	0.130	0.088	2582	1742	46.6%	0.54	1.17
56	8.634E-05	0.104	0.036	1821	1207	189.4%	0.77	3.36
57								
58	4.876E-05	0.073	0.042	2348	1507	76.2%	0.64	1.74
59	5.727E-05	0.075	0.031	2191	1312	143.2%	0.75	3.06
60	9.068E-05	0.181	0.147	2546	1992	23.1%	0.36	0.57
61	7.548E-05	0.088	0.024	1894	1170	270.4%	0.83	5.00
62	6.728E-05	0.095	0.051	2091	1410	86.8%	0.64	1.77
63	2.227E-05	0.028	0.010	2427	1277	193.1%	0.82	4.57
64	7.428E-05	0.113	0.068	2194	1516	64.5%	0.58	1.38
65	6.881E-05	0.083	0.027	1898	1202	212.0%	0.80	3.93
66								
67								
68	4.913E-05	0.092	0.070	2555	1878	31.8%	0.44	0.79
69	7.569E-05	0.091	0.031	1759	1198	188.5%	0.76	3.23
70	6.135E-05	0.100	0.057	2860	1623	74.1%	0.67	2.07
71								
74								
75	8.872E-05	0.134	0.076	2394	1514	77.1%	0.64	1.80
76	6.894E-05	0.092	0.039	2247	1335	134.0%	0.75	2.94
77	6.206E-05	0.118	0.094	2433	1902	25.5%	0.38	0.61
79	7.844E-05	0.093	0.027	1895	1185	239.9%	0.82	4.44
80	5.760E-05	0.091	0.055	2438	1580	65.0%	0.61	1.55
84	6.434E-05	0.096	0.053	2326	1484	80.7%	0.65	1.83
90	6.882E-05	0.086	0.030	2116	1252	184.7%	0.79	3.81
91	7.354E-05	0.084	0.021	1753	1145	295.0%	0.83	5.04
92	8.229E-05	0.092	0.023	1579	1124	299.4%	0.82	4.61
93								
95	6.000E-05	0.118	0.092	2642	1965	27.9%	0.42	0.72
97	5.705E-05	0.117	0.093	2795	2055	26.3%	0.42	0.72
98	7.857E-05	0.144	0.107	2499	1827	34.4%	0.46	0.84
100								
103	7.107E-05	0.138	0.114	2382	1940	20.8%	0.33	0.48
105								
106	6.833E-05	0.110	0.068	2529	1613	63.2%	0.61	1.56
107	1.004E-04	0.152	0.086	2393	1512	77.4%	0.64	1.81

4. SUMMARY

Core samples were collected from the seabed at 80 sites throughout Port Phillip Bay, and analysed for a variety of physical properties of importance in the transport processes of bed sediments.

Grain sizes were measured by fall velocity techniques, and displayed the expected distribution of fine, muddy sediments from the Central Bay and Geelong Arm, with coarser material predominating at sites nearer shore.

Sediment and bulk densities in the top 5 cm of the core samples showed wide variation between sampling sites, as did the derived quantities of water content and void. Low densities were found at the Central Bay and Geelong Arm sites. A limited number of measurements deeper in the core showed little consistent pattern in the depth variation of sediment and bulk density, but the water content and void ratio were both found to decrease with depth.

Permeabilities ranged from 1 to 0.0003 mm/s, the highest values surprisingly occurring at Central Bay sites with relatively fine grain sizes. No significant correlation was found between permeability and either grain size or porosity.

Viscosity measurements were made on samples from the top 5 cm at 46 of the sites. Flow curves typically showed higher shear stresses on the down-ramps than on the up-ramps. Yield stresses from 7 to 400 Pa were obtained.

5. ACKNOWLEDGMENTS

The core analysis program was initiated by Dr Willem de Lange and Dr Vicki Moon of the University of Waikato Earth Sciences Department, and conducted at VIMS by John Turnbull, David Hatton, David Ball, Robert Noyes-Fitzsimmons, Wei Zhou and Catherine de la Cour. The sample collection was conducted by Melbourne Water staff Shayne Wilde, Mark Bonaccurso and Russell Barrett, with diving assistance from Les Cameron, Stefan Axelsen and Graeme Meek.

Funding was provided by Melbourne Water through the Port Phillip Bay Environmental Study.

6. REFERENCES

Beasley, A. W (1966) Port Phillip Bay survey 1957-63: bottom sediments of Port Phillip Bay. Mem. Nat. Mus. Victoria, **27**: 69-105.

Berlamont J. E, Van Den Bosch L and Toorman E. (1992). Effective stresses and permeability in consolidating mud. In: *Proc 23rd Conf on Coastal Eng*, Venice, ASCE, pp. 2962-2975.

Berlamont, J., Ockenden, M., Toorman, E. and Winterwerp, J. (1993) The characterisation of cohesive sediment properties. In: H. J. de Vriend (Editor), Coastal Morphodynamics: Processes and Modelling. *Coastal Eng*, **21**: 105-128.

Black, K.P. and Rosenberg, M.A. (1991) Suspended load at three time scales. *Coastal Sediments '91*. Waterway, Port, Coastal and Ocean Div. (ASCE). **1**: 313-327.

Gibbs, R.J, Matthews, M.D. and Link D.A. (1971) The relationship between sphere size and settling velocity *J Sed Petrology*, **41**: 7-18.

Migniot, C. (1968) Study of the physical properties of different very fine sediments and their behaviour under hydrodynamic action. Houille Blanche, **7**: 591-620.

Migniot, C. and Hamm, L. (1990) Consolidation and rheological properties of mud deposits. In *Proc Conf on Coastal Eng*, Delft, ASCE, pp. 2975-2983.

Otsubo, K. and Muraoka, K. (1988) Critical shear stress of cohesive bottom sediments. *J Hydraulic Eng*, ASCE, **114**: 1241-1255.

Todd, D.K. (1959) *Ground water hydrology*. John Wiley and Sons, New York.